SYNTHESIS, CHARACTERIZATION, AND ELECTROKINETIC PROPERTIES OF POLYINDENE/COLEMANITE CONDUCTING COMPOSITE

Berrak Cetin, Halil Ibrahim Unal*, and Ozlem Erol

Smart Materials Research Lab, Department of Chemistry, University of Gazi, Ankara, Turkey

Abstract—The aim of the aqueous electrokinetic experiments in the present study was to assess the relative contribution of the conducting polyindene (PIn) and inorganic colemanite components to the zeta (ζ) potentials of the composite particles, thus providing further insight into their surface composition in the dispersed state and establishing colloidally stable conditions for potential rheological, industrial applications. For this, PIn and a PIn/colemanite composite (containing 5 wt.% colemanite) were synthesized by chemical oxidative polymerization using $FeCl_3$ as an oxidizing agent. Colemanite, PIn, and PIn/colemanite composite samples were characterized by Fourier-transform infrared spectroscopy, elemental analysis, conductivity, dielectric constant, magnetic susceptibility, density, particle-size measurements, thermogravimetric analysis, differential scanning calorimetry, X-ray diffraction analysis, and scanning electron microscopy methods. The electrokinetic properties of colemanite and PIn/colemanite composite dispersions were determined by ζ-potential measurements in aqueous medium, taking into account the effects of time, pH, various electrolytes, surfactants, and temperature. The pH was observed to have a greater effect on the ζ potentials of colemanite in water but caused only slight changes in the presence of cationic ($NaCl$, $BaCl_2$, $AlCl_3$) and anionic ($NaCl$, Na_2SO_4) electrolytes. Increased pH values shifted the ζ potentials of PIn/colemanite composite dispersions to more negative values. The most effective surfactant acting on the ζ potentials of colemanite and PIn/colemanite composite dispersions was cetyltrimethylammonium bromide (CTAB), which shifted the ζ potentials to more positive regions. Elevated temperatures caused almost no change to the ζ potentials of either the colemanite or the PIn/colemanite composite dispersions.

Key Words—Colemanite, Conducting Composite, Electrokinetics, Polyindene.

INTRODUCTION

Synthesis of composite materials by combining organic and inorganic interfaces at a molecular level is very interesting scientifically. The organic component of the composite offers structural flexibility, convenient processing, and tunable electrical and electronic properties. The inorganic component of the composite provides a potential for high carrier mobilities, band-gap tunability, thermal and mechanical stabilities, and a range of electric, magnetic, and dielectric properties. A major attraction of such research activities is to combine these properties in organic/inorganic hybrid materials, which can then be improved in comparison to the inherent properties of each of the separate components (Walcarius, 2001; Mitzi, 2001).

Intrinsically conducting polymers, also known as "synthetic metals," are polymers with highly π-conjugated polymeric chains (Lu *et al.*, 2011) which are insufficient to be conductive, and which need dopant ions to become so (MacDiarmid, 2001; Oyhenart *et al.*, 2005). Many monomers have been used for the synthesis of conducting polymers such as aniline, thiophene, pyrrole, and indene. In the PIn structure, the phenyl

rings line up in planar fashion which explains why repeated monomers create an almost planar structure. The unique construction of PIn ensures a high glass-transition temperature (T_g) and this property has increased its popularity among researchers (Kanaoka *et al.*, 2002).

Western Turkey possesses the largest boron deposits in the world and the most important minerals are tincalconite ($Na_2O.2B_2O_3.5H_2O$), ulexite ($Na_2O.2CaO.5B_2O_3.16H_2O$), and colemanite ($2CaO.3B_2O_3.5H_2O$) (Gemici *et al.*, 2008; Kavas *et al.*, 2011). Colemanite is a primary boron derivate containing silica, calcium, and boron. The basic structure of colemanite contains endless chains of interlocking $BO_2(OH)$ triangles and $BO_3(OH)$ tetrahedrons with calcium, crystalline water molecules, and extra hydroxides interspersed between the chains (Sari and Tuzen, 2009). The sheets are held together by weak hydrogen bonds involving both water molecules and hydroxyl groups (Hancer and Celik, 1993).

The electrokinetic potential on a surface of a solid particle in contact with a polar medium (*i.e.* H_2O) is controlled by the dissociation of surface groups, the preferential adsorption and isomorphic substitution of cations or anions, the adsorption of polyelectrolytes or surfactants, and the accumulation or depletion of electrons. Generally, descriptions of the charge distribution at solid/liquid interface assume the presence of an

* E-mail address of corresponding author:
h.i.unal@gmail.com

electrical double layer consisting of a fixed layer (Stern) and a diffuse layer. Externally applied electrical forces cause a relative movement between these layers. The potential at this surface is called the electrokinetic or zeta (ζ) potential. In an aqueous solution, the electrokinetic properties of fine particles, such as the isoelectric point (IEP) and potential-determining ions, play a significant role in understanding the adsorption mechanism of inorganic and organic species at the solid/liquid interface. These electrokinetic properties also govern the flotation, coagulation, and colloidal properties in various dispersion systems (Hang *et al.*, 2007).

Molecules and particles that have sufficiently large ζ-potential values (negative or positive) in dispersions will show colloidal stability. When the ζ potential of dispersed particles is small, the attractions of suspended particles to each other overcome the repulsive forces and tend to agglomerate. Some parameters such as time, pH, temperature, and ion and surfactant concentrations and types may affect the values of ζ potentials.

The interface between a solid and a solution may be treated as a semi-permeable membrane which allows only the charged species common to both the solid and the solution. These charged species are referred to as potential-determining ions and have the ability to affect the sign of the ζ potential. Potential-determining ions are the major ions responsible for establishing the surface charge of particles (Celik, 2004; Duman and Tunc, 2009). Some ions, referred to as "indifferent," are adsorbed by electrostatic attraction, thereby only affecting the magnitude of the ζ potential (Rao, 2004). The indifferent ions remain within the outer part of the electrical double layer (diffuse) and do not adsorb strongly at the wall of the solid particle (Duman and Tunc, 2009).

In the present study, polyindene/colemanite conducting composite fine particles were prepared to combine and improve upon the advanced properties of the two original materials, and the properties of the new composites were characterized by a number of means. The effects of various parameters on the electrokinetic properties in aqueous colloidal dispersions were investigated. The resultant conducting composite particles were then used in an electro-rheological (large change in viscosity upon the application of an external electric field), vibration-damping study.

EXPERIMENTAL

Materials

A sample of colemanite (ideal stoichiometry of $2CaO.3B_2O_3.5H_2O$) was supplied by ETI Mining Co. (Ankara, Turkey) and had the following composition: B_2O_3 (27%), CaO (26%), SiO_2 (13%), MgO (6%), Al_2O_3 (0.5%), SrO (1.5%), Fe_2O_3 (0.4%), Na_2O (0.6%), SO_4 (1%), As (70 ppm), and loss on ignition (24%). Anhydrous $FeCl_3$, $CHCl_3$, and all the other reagents,

which were of analytical grade, were supplied by Merck (Darmstadt, Germany) and used as received. Indene (supplied by Merck) was subjected to vacuum distillation before use.

Synthesis of Polyindene

Polyindene (PIn) was synthesized by chemical oxidative polymerization. For the synthesis, 0.02 mol of $FeCl_3$ was dispersed in 40 mL of $CHCl_3$ and stirred continuously under $N_{2(g)}$ atmosphere at $15-20^{\circ}C$. Freshly distilled indene (0.01 mol) was added dropwise to this dispersion and stirred continuously at the same temperature for a further 5 h. After recovering the crude PIn, it was filtered and washed thoroughly several times with distilled hot water and ethanol to remove any impurities present (*i.e.* unreacted initiator, monomer, oligomer), dried in a vacuum oven at $70^{\circ}C$ for 24 h, and recovered with a 94% yield. The PIn synthesized was used for Fourier-transform infrared spectroscopy (FTIR), differential scanning calorimetry (DSC), and particle-size measurements. Other data for PIn were taken from a previous study and cited where appropriate (Guzel *et al.*, 2012).

Synthesis of a PIn/colemanite composite

The PIn/colemanite composite was synthesized using $FeCl_3$ as an oxidizing agent by *in situ* chemical oxidative polymerization. The molar ratio of oxidant to monomer was again taken as 2:1. Colemanite (0.31 g, previously milled and dried in a vacuum oven at $50^{\circ}C$) and $FeCl_3$ (0.12 mol) were dispersed in 250 mL of $CHCl_3$ in a three-necked flask and then stirred for 20 min under $N_{2(g)}$ atmosphere at $15-20^{\circ}C$. Next, freshly distilled indene (0.06 mol, previously dispersed in $CHCl_3$) was added dropwise to the flask. The reaction was carried out under $N_{2(g)}$ atmosphere at $15-20^{\circ}C$ for 5 h. The precipitate of PIn/colemanite composite was washed with ethanol to remove any impurities present, dried in a vacuum oven at $70^{\circ}C$ for 24 h, recovered with 82% yield, and then characterized.

Characterization

Colemanite and PIn/colemanite were ground using a Retsch MM400 model milling machine (Haan, Germany) for 20 min at 30 Hz and characterized as follows.

FTIR spectra of the samples compressed with KBr discs were recorded using a Mattson-1000 model spectrometer (Humberside, UK) (KBr:sample ratio 100:1). The resolution for the FTIR spectra was 0.4 cm^{-1}, and 20 scans were collected for each spectrum.

The average particle sizes of the samples prepared in deionized water were determined by photon correlation spectroscopy using a Malvern Zetasizer Nano-ZS (Worcestershire, UK) equipped with a 4 mW He-Ne laser operating at $\lambda = 633$ nm and non-invasive back-scatter (NIBS$^{\text{TM}}$, angle of 173°) optics (Worcestershire,

UK). The autocorrelation function was analyzed using the Malvern dispersion technology software supplied by the manufacturer (NanoApplication.exe) to obtain the particle size (Tkachenko *et al.*, 2006).

Solid pellets of samples were prepared as compressed discs (thickness: 0.5 cm × diameter: 1.3 cm) and used for density, conductivity, and dielectric-constant measurements.

The conductivities of the samples were determined using a four-probe technique with a FPP-460A model four-probe device (Entek Electronik Co., Ankara, Turkey). The DC conductivity of the materials was measured by the Standard van der Pauw four-probe method (Van der Pauw, 1958) and the capacitance of the materials was measured using an HP 4192 A LF Impedance Analyzer at f = 1 MHz and the dielectric constants calculated according to the equation: $C = \varepsilon_o \varepsilon A/d$, where C is the capacitance, ε_o is the dielectric constant of free space, ε is the dielectric constant of the sample, A is the surface area of the sample, and d is the thickness of the sample (Agilent Technologies, Berkshire, UK). All the measurements were taken with the help of a microcomputer through an IEEE-488 ac/dc converter card.

A Sherwood Scientific MKI Model Gouy balance (Cambridge, UK) was used to determine the magnetic susceptibility of the samples at ambient temperature. Finely powdered polymer samples were placed in a glass tube at a height of not less than 2.5 cm. This glass tube was placed in the hole of the magnetic balance, which was on a wooden bench, to obtain a constant value.

Elemental analysis of the PIn/colemanite composite was performed using a LECO CHNS-932 analyzer (Michigan, USA) (Matejovic, 1993); the Fe content of the composite was determined using a Varian model AA240FS atomic absorption spectrometer (Palo Alto, California, USA), equipped with an iron hollow-cathode lamp, a deuterium lamp for background correction, and an air-acetylene flame as the atomizer. The apparatus was run under the conditions suggested by the manufacturer, *i.e.* lamp current, 9.0 mA; wavelength, 248.3 nm; bandwidth of the slit, 0.5 nm; acetylene flow rate, 1.0 L min^{-1} (Yalcinkaya *et al.*, 2010); and the boron content was determined using a Hach DR2800 spectrophotometer (Loveland, Colorado, USA) (Gupta and Stewart, 1975).

Thermogravimetric (TGA) analyses of the samples were performed using a TA Instruments-Q500 model thermogravimetric analyzer (New Castle, Delaware, USA) under $N_{2(g)}$ atmosphere up to 900ºC, at a heating rate of 10ºC min^{-1} in a platinum sample holder; and DSC experiments were carried out using TA Instruments-Q-2000V.24.4 Build 116 (New Castle, Delaware, USA).

The powdered form of the samples was used for XRD experiments using a PANalytical MPD X-ray diffractometer (Almelo, The Netherlands) with CuKα radiation

(λ = 0.51406 nm at 40 mV and 40 mA). Data were collected over the range 10−50º2θ at a scan rate of 0.6º2θ min^{-1}. The morphologies of the samples were investigated using an FEI Quanta 200F scanning electron microscope (SEM) (Hillsboro, Oregon, USA). The samples were mounted on specimen stubs with double-sided adhesive tape, and coated with gold using a Polaron SC 502 sputter coater for examination, prior to SEM observation.

ζ-potential measurements of colloidal dispersions

The ζ potentials of colloidal dispersions were measured using a Malvern Zeta-Sizer Nano-ZS ζ-potential analyzer which works with a laser doppler electrophoresis technique. The optic unit contains a 4 mW He-Ne laser (λ = 633 nm). The self-optimization routine (laser attenuation and data-collection time) in the Zeta-Sizer software was used for all the measurements. In an aqueous medium, the ζ potential was calculated from the electrophoretic mobility using the Smoluchowski model where the thickness of the electrical double layer (κ^{-1}) is assumed to be smaller than the dispersed-particle size (Stamm, 2008):

$$\zeta = \frac{\eta U_E}{\varepsilon} \tag{1}$$

where U_E is the electrophoretic mobility, ε is the dielectric constant of the medium, and η is the viscosity of the medium. The electrophoretic mobility was obtained by performing an electrophoresis experiment on each of the samples and the velocity of the dispersed particles was measured using a laser doppler velocimeter. The colloidal dispersions of the samples with a concentration of 0.1 g L^{-1} were prepared in deionized water for ζ-potential measurements. Then, each of the dispersions was subjected to ultrasonication for 30 min and held at room temperature for a further 2 h to establish equilibrium. Afterwards, the supernatant liquid was used for ζ-potential measurements and the pH was adjusted immediately using an MPT-2 autotitrator unit at 25ºC. In this manner, the effects of time, pH, various electrolytes [(cationic: NaCl (monovalent, 0.01 M), BaCl$_2$ (divalent, 0.01 M), AlCl$_3$ (trivalent, 1 × 10^{-4} M), anionic: NaCl (monovalent, 0.01 M), Na$_2$SO$_4$ (divalent, 0.01 M)], surfactants (cationic: cetyltrimethylammonium bromide (CTAB), anionic: sodium dodecyl sulfate (SDS), non-ionic: Triton-X 100), and temperature on the ζ potentials of the colemanite and PIn/colemanite colloidal dispersions were investigated and the colloidal stabilities determined.

RESULTS AND DISCUSSION

Characterization results

The FTIR spectrum of colemanite indicated absorption at 3603 cm^{-1} which arose from free O−H stretching vibrations (Figure 1a). The broad peak above 3000 cm^{-1}
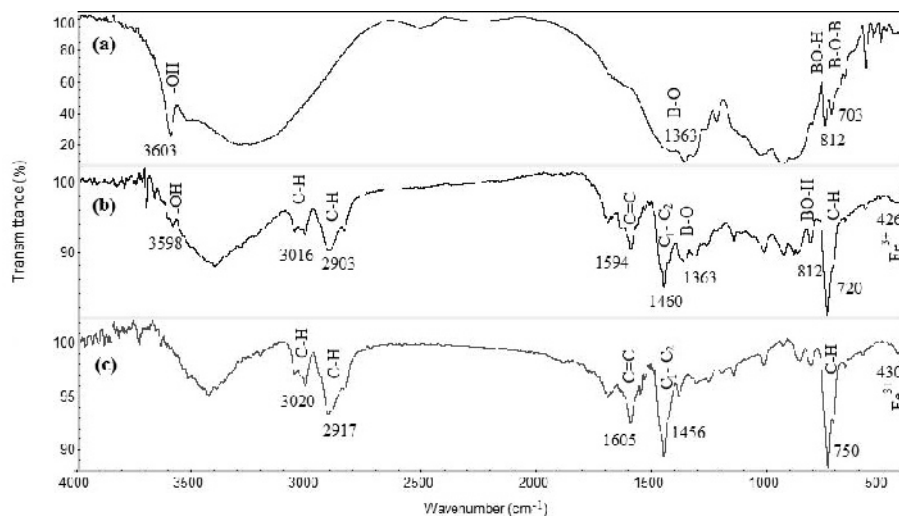
Figure 1. FTIR spectra of samples (a) colemanite, (b) PIn/colemanite, and (c) PIn.

can be attributed to crystalline water present in the structure of colemanite. The peak at 1363 cm^{-1} can be attributed to B$-$O stretching vibrations and the peaks at 812 cm^{-1} and 703 cm^{-1} can be attributed to B$-$O$-$H and B$-$O$-$B twistings, respectively (Weir, 1966; Pavlyukevich et al., 2009; Park et al., 2007). The FTIR spectrum of PIn showed peaks at 3020 cm^{-1} arising from aromatic C$-$H stretching vibrations and at 2917 cm^{-1} due to aliphatic C$-$H stretching vibrations (Figure 1b). The peaks at 1605 and 1456 cm^{-1} can be attributed to aromatic $-$C=C vibrations and C$_1$$-C_2$ bending vibrations, respectively (Kennedy et al., 1993). The FTIR spectrum of the PIn/colemanite composite (Figure 1c) showed peaks at 3598 and 1363 cm^{-1} which can be attributed to $-$OH stretching vibrations and B$-$O deformation and stretching vibrations of colemanite, respectively; peaks at 3016, 2903, 1594, and 1460 cm^{-1} can be attributed to the aromatic C$-$H and aliphatic C$-$H stretching vibrations, bending vibrations of aromatic $-$C=C, and bending vibrations of C$_1$$-C_2$ of the PIn structure, respectively. The peak at 750 cm^{-1} is due to the out-of-plane aromatic C$-$H stretching vibrations. Cakic et al. (2002) reported that the peaks at 1632 and 450 cm^{-1} can be attributed to Fe(III) complexes. The peaks at 426 cm^{-1} (Figure 1c) and at 430 cm^{-1}

(Figure 1b) can be attributed to the iron complexes such as [FeCl$_4$]$^-$ which are the remaining electrostatically dopant counter anions in the vicinity of PIn chains. The FTIR spectra proved that the PIn/colemanite composite had been synthesized successfully.

Physical data for colemanite, PIn, and the PIn/colemanite composite (Table 1) confirmed that particle-size distribution is an important parameter for colloidal stability against gravitational sedimentation. The particle sizes of the samples were measured by both dynamic light scattering (DLS) and scanning electron microscopy (SEM) (Figure 2) techniques. The hydrodynamic diameters of the samples measured by DLS were greater than those measured by SEM, as expected (DLS gives hydrodynamic size and SEM gives bare particle size). The diameter of particles in the PIn/colemanite composite was greater than those in both PIn and colemanite, which may be attributed to the surrounding of the colemanite particles by PIn chains. The inclusion of PIn chains in the colemanite structure also caused reduction of the density of PIn/colemanite composite, determined by weighing the mass of the disc-shaped sample pellets and calculating the volume of a cylinder.

The dielectric constant values were proportional to their conductivities (Table 1), as also reported by Ulgut

Table 1. Physical properties of the samples.

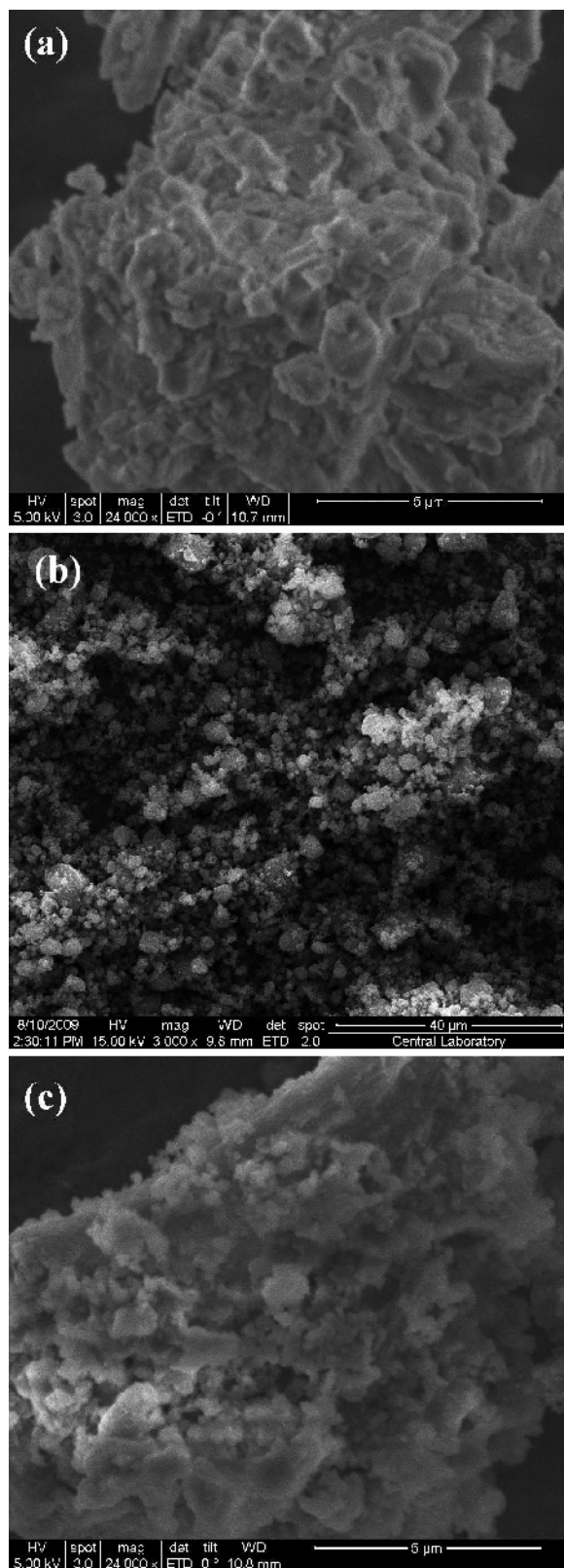| Samples	Hydrodynamic diameter (DLS, μm)	Average diameter (SEM, μm)	Apparent density (g cm^{-3})	Dielectric constant (at 1 MHz)	Magnetic susceptibility (X_g, cm^{3}g^{-1}) $\times 10^6$	Conductivity (S cm^{-1}) $\times 10^4$
Colemanite	1.2	0.84	1.69	85	-1.1	3.14
PIn	1.4	1.10	0.91	74	3.5	1.85
PIn/colemanite composite	2.2	1.40	1.02	83	-0.8	2.48

Figure 2. SEM images of (a) colemanite, (b) PIn, and (c) PIn/colemanite.

et al. (2009) on a study carried out on poly(3,4-ethylenedioxythiophene), poly-3-hexylthiophene, and polypyrrole conducting polymers. The conductivity value of the PIn/colemanite composite was between the conductivity values of colemanite and PIn. The B_3O_3 hexagonal rings of colemanite are connected by $-B-O-B-$ bonds (Figure 3). Two triangles made up of two B_2O_3 molecules formed between these two rings increase the electronegativity of the colemanite structure. The electron density of the composite increased due to the empty bands in the rings of B_3O_3 hexagonal rings and this resulted in the enhanced conductivity of PIn/colemanite composite. This conclusion is supported by the results reported (El-Desoky, 2003) on the dc conductivity and the hopping mechanism in V_2O_5-B_2O_3-BaO.

The magnetic susceptibility of PIn was reported to be positive (Guzel *et al.*, 2012), whereas colemanite (Alp, 2008) and PIn/colemanite were negative, indicating that PIn was paramagnetic and colemanite and PIn/colemanite composite were diamagnetic. As a result, the conductivity mechanisms of PIn and PIn/colemanite were polaron and bipolaron in nature, respectively.

The theoretical and experimental compositions obtained from elemental analysis of the PIn/colemanite composite are [87.4% C, 7.3% H, and 2.49% B_2O_3] and [85.51% C, 5.37% H, 2.57% B_2O_3, and 0.8% Fe], respectively. The percentage of colemanite in the PIn/colemanite composite was calculated as 5.15% from the elemental analysis. The results are consistent with the expected values and indicated the successful formation of the PIn/colemanite conducting composite structure as intended. The results also indicate that residual amounts of iron were present in the composite because of the presence of $[FeCl_4]^-$ dopant counter anions.

The SEM image of colemanite (Figure 2a) revealed a dispersed and porous structure, which is in agreement with the technical literature reported for colemanite (Atar and Olgun, 2007; Davies *et al.*, 1991). The PIn (Figure 2b) had a granular, porous, and sponge-like morphology, as reported by Cabuk *et al.* (2010) and by Eristi *et al.* (2007). The SEM image of the PIn/colemanite composite (Figure 2c) revealed that porous structures of colemanite particles were surrounded homogeneously by close-packed PIn chains, which supported the successful formation of the PIn/colemanite composite.

The XRD pattern of colemanite showed sharp peaks at 15, 23, 28, 35, and 45º2θ, besides showing peaks of dolomite, calcite, smectite, and quartz, which is consistent with the composition results given in the experimental section (Figure 4a). The XRD pattern of colemanite was in agreement with those given in the literature (Gur, 2007; Ucar and Yargan, 2009). The XRD pattern of the PIn/colemanite composite showed sharp peaks at 15, 22, and 28º2θ (Figure 4c) with lower intensities than the colemanite. This indicated that the
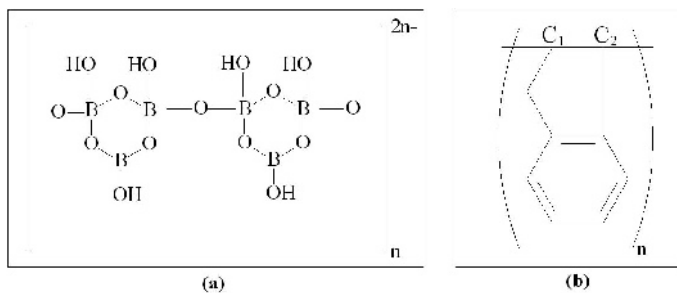
Figure 3. The structures of (a) colemanite and (b) PIn.

amorphous structure of PIn (Figure 4b), which is dominant (~95%), covered the crystalline structure of colemanite (~5%).

In the TGA curve of colemanite, two-step weight losses at 395 and 680ºC were observed (Figure 5). The first step at 395ºC was attributed to the removal of structural hydroxyl groups as water molecules and breaking of H bonds between water and borate chains. The second step (680ºC) corresponded to the removal of lattice water, typical of crystalline substances and also
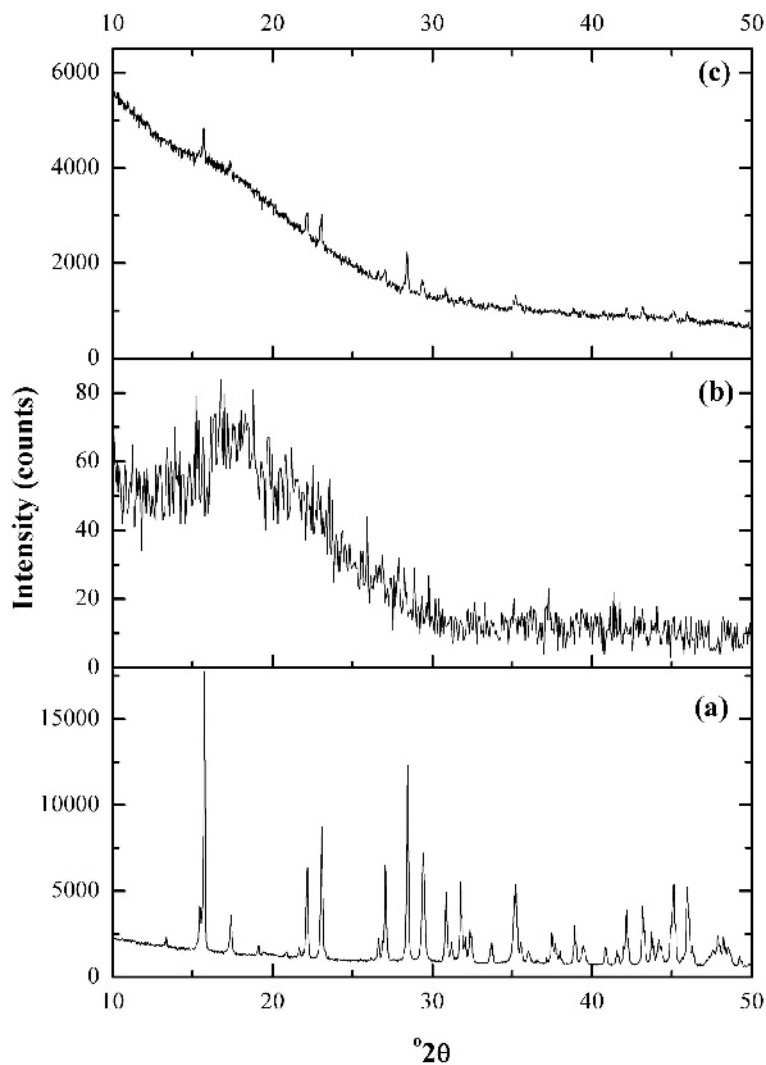
Figure 4. XRD patterns of (a) colemanite, (b) PIn, and (c) PIn/colemanite.

Table 2. TGA results from the respective samples.

Samples	— Degradation temperatures (ºC) —			Residue at 900ºC (w/w%)
	$*T_i$	$*T_m$	$*T_f$	
Colemanite	395	416	436	75
	680	710	740	
PIn	340	375	404	28
PIn/colemanite composite	420	465	512	5

$*T_i$, initial degradation temperature; T_m, maximum degradation temperature; T_f, final degradation temperature.

supported by the data of Waclawska and Stoch (1988) and Kaynak and Isitman (2011) on thermal decomposition of colemanite and colemanite/polystyrene fire retardant composite, respectively. Thermal decomposition of PIn started at 340ºC, which corresponded to the breaking of chemical bonds between PIn chains, and ended with 72% weight loss (Figure 5). The thermal stability of polypyrrole/PIn was investigated by Bozkurt *et al.* (1996) who reported 80% weight loss for PIn. The thermal behaviors of acrylonitrile/PIn copolymers were also investigated by Sabaa *et al.* (1989) under air atmosphere and almost 100% weight loss was reported for PIn. The TGA curve of PIn/colemanite composite (Figure 5) showed one-step decomposition with initial decomposition temperature of 420ºC and the final decomposition temperature of 512ºC, corresponded to the removal of hydroxyl groups from colemanite as water molecules, the breaking of H-bonds between borate and water molecules as well as the decomposition of PIn chains. The initial decomposition temperatures of samples were as follows (Table 2): $T_{i(PIn/colemanite)}$ (420ºC) > $T_{i(colemanite)}$ (395ºC) > $T_{i(PIn)}$ (340ºC). According to these values, the thermal stability of the PIn/colemanite composite was greater than the thermal stabilities of either colemanite or PIn, as was the aim.

The DSC thermogram of colemanite (Figure 6a) revealed two sharp endothermic peaks at 378 and 397ºC, which corresponded to the removal of crystalline water, and supported by Kaynak and Isitman (2011). The DSC thermogram of PIn (Figure 6b) showed a shoulder at 178ºC and an endothermic transition peak at 370ºC which corresponded to T_g (Soga and Monoi, 1989; Kennedy *et al.*, 1993) and the decomposition of PIn chains, respectively. The DSC thermogram of the PIn/colemanite composite (Figure 6c) showed one shoulder at 189ºC and an endothermic peak at 361ºC which were attributed to the T_g of PIn chains and to the removal of the crystalline water of colemanite, respectively. The difference between T_g values of PIn may be attributed to the differences between molecular weights of free PIn chains and PIn chains in the composite structure and also to the secondary forces acting between PIn chains and colemanite particles.

Electrokinetic studies

The electrokinetic properties of the materials were determined by ζ-potential measurements in an aqueous medium and the results obtained are discussed below.

Effect of time on pH. Colemanite comprises $[B_3O_4(OH)_3]_n^{2n-}$ polyanions or equivalent forms of $[B_4O_7.2H_2O]^{2-}$ groups. The polymeric structure of colemanite is formed by B–O–B bridges which are joined laterally by calcium to form sheets *via* ionic bonding. To determine the pH profile of colemanite, PIn, and PIn/colemanite composite colloidal dispersions ($c = 0.1$ g L^{-1}), the changes in pH with time were investigated (Figure 7). For dispersion of colemanite, the initial pH value was measured at 8.7, increased to 9.2 in 2 min, and remained stable thereafter. This may be attributed to the adsorption of H_3O^+ ions on the surfaces of negatively charged colemanite particles, increased concentration of OH^- ions in the dispersion medium, and dissolution, over time, of colemanite which has an amphoteric nature and the solubility of which is ~0.8 g L^{-1}, as reported by Hancer and Celik (1993). The equilibrium pH values of colemanite were reported to be 9.3 by Celik *et al.* (2002) and between 9.1 and 9.4 by Ucar *et al.* (2009). The initial pH of PIn was reported to be 5.9 and reached 5.7 after 120 min (Guzel *et al.*, 2012). For the PIn/colemanite composite dispersion, the
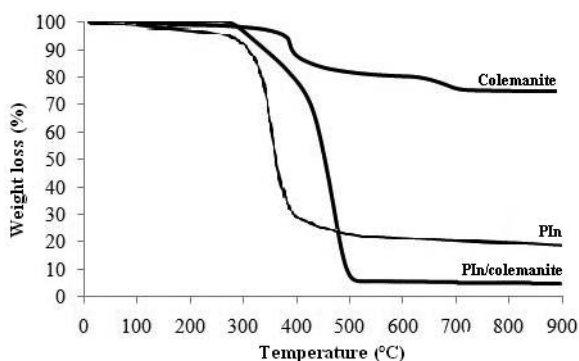

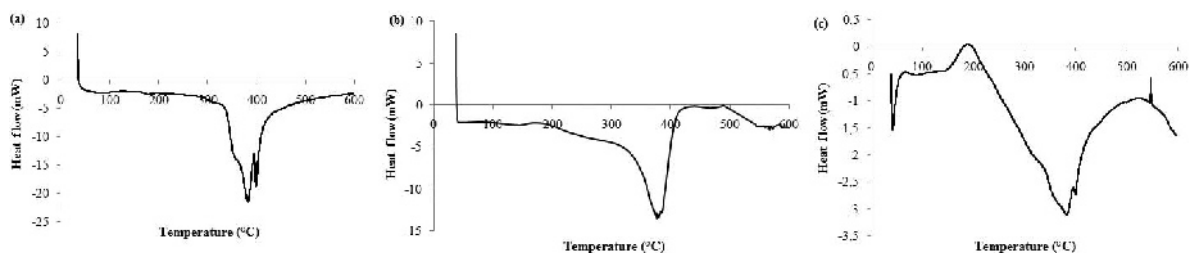
Figure 5. TGA curves of the samples.

Figure 6. DSC curves of (a) colemanite, (b) PIn, and (c) PIn/colemanite.

initial pH value was measured at 7.9 and reached 6.8 after 60 min. This pH decrease may be attributed to the exchange of dopant anions $[FeCl_4]^-$ with OH^- anions in the dispersion as in the case of PIn (Guzel *et al.*, 2012). On the other hand, the equilibrium pH value of PIn/colemanite was greater than that of PIn due to the presence of colemanite in the composite structure. Colemanite and PIn/colemanite composite samples are assumed to have reached ionic equilibrium after 120 min. Thus, for the rest of the ζ-potential measurements, the colloidal dispersions were prepared and held for 120 min before carrying out the subsequent ζ-potential measurements.

Effect of pH on ζ potentials. The effect of pH on ζ potentials of colemanite, PIn, and PIn/colemanite composite (Figure 8, Table 3) revealed that the ζ-potential values of colemanite fell into the negative region and changed in a relatively narrow range ($\zeta_{pH = 2.2}$ = −9 mV and $\zeta_{pH = 11.1}$ = −21 mV) without showing an IEP. At lower pH values, the ζ potential of colemanite was shifted to more positive values because of the adsorption of H_3O^+ ions onto the negatively charged surfaces of colemanite particles. With the addition of base solution into the dispersion medium, OH^- anions increased the number of negative charges present and, as a result, the ζ-potential values shifted to more negative regions. Such behavior is inconsistent with the data

reported in the literature, in which the IEP value of colemanite was observed at ~pH 10 (Hancer and Celik, 1993; Celik and Bulut, 1996; Ucar and Yargan, 2009; Ozdemir and Celik, 2010; Sahinkaya and Ozkan, 2011). The variations in IEPs were attributed to the heterogeneity of mineral surfaces, to the presence of impurities, and to various pretreatments such as leaching, washing, ultrasonic scrubbing, and sludge removal. The differences between cited values for IEP and the results from the present study may be attributed to mineral heterogeneity (*i.e.* the presence of 13% silica in colemanite) which influences the surface properties of the dispersed particles measured by electrophoresis (Celik and Bulut, 1996; Ozdemir and Celik, 2010). The values of the IEPs of silica are reported to be usually in the strongly acidic region (Parks, 1965) and the reported values vary between 1.5, 2.8, and 0 (Tang *et al.*, 2005; Lee *et al.*, 2007). The ζ-potential profile of colemanite was assumed to become similar to the ζ-potential profile of silica when dispersed in aqueous medium, which may be a result of the covering of the surfaces of colemanite particles by silica particles in the colloidal dispersion.

The changes in ζ potential with pH for PIn were taken from a previous study by the present authors to compare with the PIn/colemanite composite (Guzel *et al.*, 2012). A large ζ-potential change and IEP (pH = 5.1) was reported for PIn dispersions. The counter dopant anions
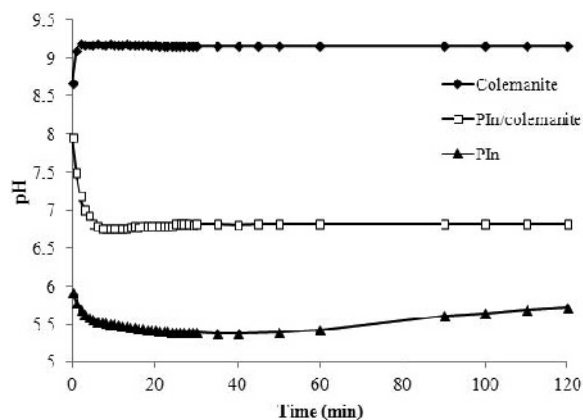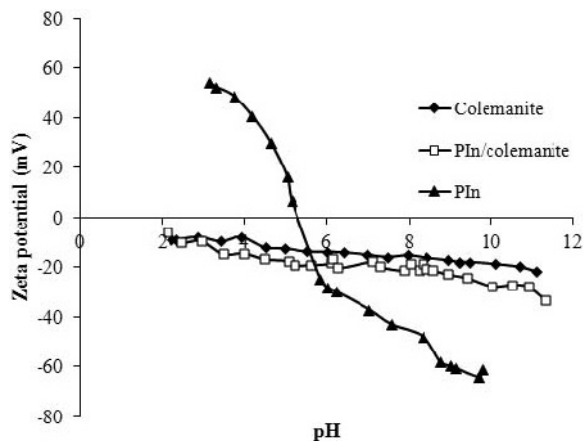

Figure 7. Change of pH with time for the samples.

Figure 8. Effect of pH on the ζ potentials of the samples

Table 3. Zeta (ζ) potential values of the samples.

Samples	Min. pH	ζ potential at min. pH (mV)	Max. pH	ζ potential at max. pH (mV)	IEP pH
Colemanite	2.2	−9.2	11.1	−21.1	−
PIn/colemanite	2.1	−5.7	11.3	−33.2	−
PIn	3.1	54.2	9.8	−61.4	5.1

of $[FeCl_4]^-$ present in the structure of PIn surrounded the PIn chains and resulted in a negative ζ-potential value of −24 mV at the initial pH of 5.71. In the present study, on the other hand, PIn/colemanite particles were negatively charged over the whole pH range examined and showed similar behavior to the colemanite; the composite consisted predominantly of PIn (94.8%). Such behavior may be attributed to the colemanite-rich (with 13% silica) surface of the PIn/colemanite composite in aqueous dispersion.

Effect of electrolytes on ζ potentials. Experiments for colemanite were carried out in only the basic region

because of the formation of boric acid in acidic medium. The effect of cationic and anionic electrolytes on ζ potentials of colemanite (Figures 9a and 9b) revealed that monovalent (Na^+) and divalent (Ba^{2+}) cations and monovalent (Cl^-) and divalent (SO_4^{2-}) anions were indifferent ions which only compressed the electrical double layer. A trivalent cation (Al^{3+}), on the other hand, was defined as a potential-determining ion for colemanite. Al^{3+} ions may exist in non-hydroxyl forms below pH 4, and begin to hydrolyze and precipitate at low pH. As pH increases above 4, hydroxyl complexes are formed, such as $Al(OH)^{2+}$, $Al(OH)_2^+$, $Al(OH)_3$, and $Al(OH)_4^-$ (Gregory, 1989). Hydroxyl complexes are very
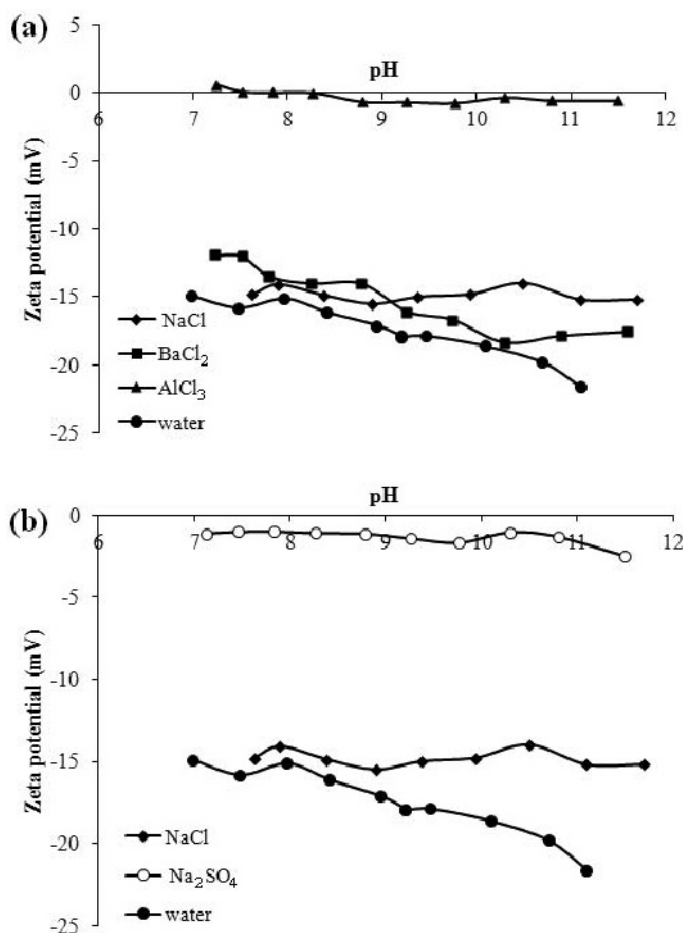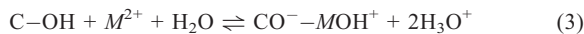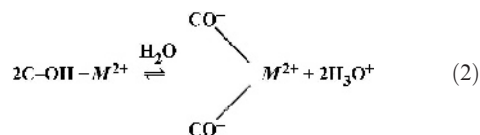

Figure 9. Effect of (a) cationic electrolytes and (b) anionic electrolytes on the ζ potential of colemanite.

surface active, adsorb strongly on negatively charged solid surfaces, and, in fact, even adsorb to positively charged surfaces (Sahinkaya and Ozkan, 2011).

The ζ-potential values shifted to the more positive region with increasing ionic valence. The ζ-potential values of the colemanite dispersion at ~pH 7 were $\zeta_{Al^{3+}} = 0.5$ mV, $\zeta_{Ba^{2+}} = -11.9$ mV, and $\zeta_{Na^+} = -14.8$ mV for cations; and $\zeta_{SO_4^{2-}} = -1.1$ mV and $\zeta_{Cl^-} = -14.8$ mV for anions. On the other hand, the ζ-potential values of colemanite dispersions in the presence of all ions except divalent cations (Ba^{2+}) did not change significantly with pH. Except for Ba^{2+}, all the ions present in the colemanite dispersions restricted the adsorption of OH^- onto the surfaces of colemanite particles and, thus, the ζ potentials became independent of pH. The surface charge of a dispersed colemanite particle (C−OH) may be a result of a combination of the following reactions, as explained for various oxide surfaces by Davis *et al.* (1978):

$$2C-OH-M^{2+} \underset{H_2O}{\rightleftharpoons} \begin{matrix} CO^- \\ \diagdown \\ \diagup \\ CO^- \end{matrix} M^{2+} + 2H_3O^+ \qquad (2)$$

$$C-OH + M^{2+} + H_2O \rightleftharpoons CO^- - MOH^+ + 2H_3O^+ \qquad (3)$$

Specific adsorption of multivalent cations almost always involves proton exchange, as indicated by reactions 2 and 3. An important characteristic of this adsorption process is the number of H_3O^+ ions released or OH^- ions adsorbed for each cation adsorbed on the surface of the particle. The fact that the H_3O^+/M^{2+} exchange stoichiometry is usually <2 means that the surface charge becomes increasingly positive, which is reflected in a change in the electrokinetic properties of the liquid−colemanite particle interface (Alkan *et al.*, 2005; Figure 9a). A similar behavior was reported by
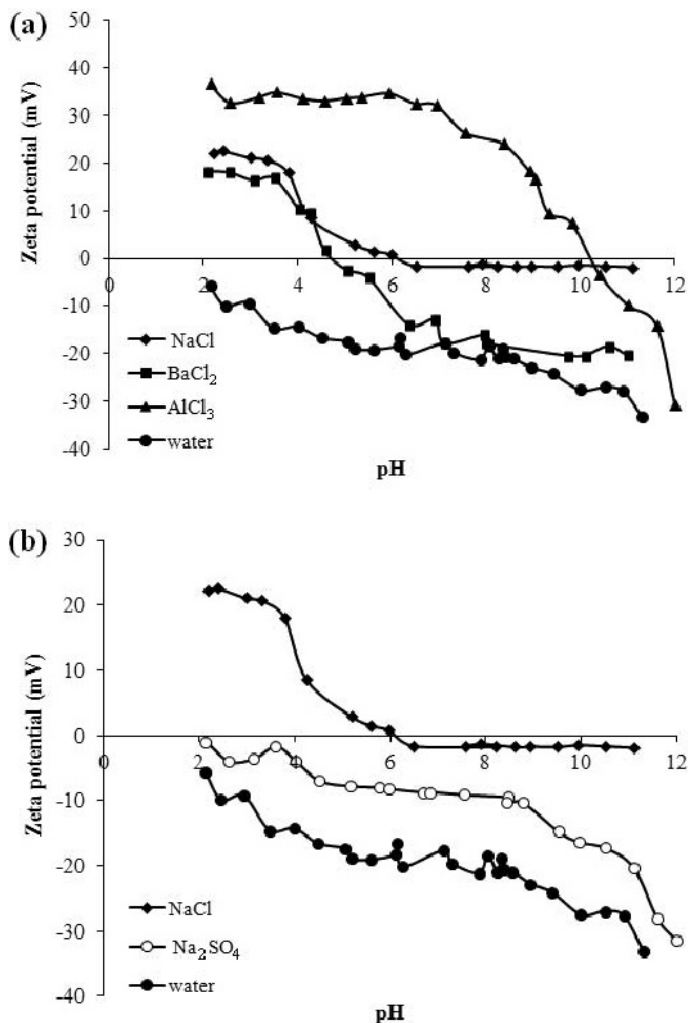

Figure 10. Effect of (a) cationic electrolytes and (b) anionic electrolytes on the ζ potential of PIn/colemanite.

Duman and Tunc (2009) for the ζ potential of Na-bentonite in divalent electrolytes. Ishikawa *et al.* (2005) also reported that the ζ potential of a kind of latex was insensitive to pH up to 8 in 0.01 M NaCl.

The results of the effects of various cationic and anionic electrolytes on ζ potentials of PIn/colemanite composite dispersions were also investigated (Figure 10). Trivalent (Al^{3+}) cations acted as potential-determining ions. Mono- (Na^+) and divalent (Ba^{2+}) cations and mono- (Cl^-) and divalent (SO_4^{2-}) anions behaved as indifferent ions for this system at the initial pH of 6.8. The ζ-potential values of PIn/colemanite shifted to positive regions with decreasing pH because of H_3O^+ adsorption in the presence of cationic electrolytes. This shift to the positive regions increased with increasing valence of the ions in the dispersion. In the presence of Ba^{2+} ions, however, the ζ-potential values remained in the less positive region, when compared to the monovalent (Na^+) and trivalent (Al^{3+}) cations (Figure 10a). This electrokinetic behavior of composite

particles may be attributed to the greater selectivity of the surface for the Ba^{2+} ion over the other cations due to its larger ionic radius. The ζ-potential values of PIn/colemanite obtained at pH 6.8 were: $\zeta_{H_2O} = -17.7$ mV, $\zeta_{Na^+} = -1.6$ mV, $\zeta_{Ba^{2+}} = -12.9$ mV, and $\zeta_{Al^{3+}} = 32.2$ mV. The cations compressed the electrical double layer and, thus, reduced the value of the ζ potential. The reason for the greatest positive ζ potential observed in the presence of Al^{3+} may be attributed to the reversed sign of the effective charge of the PIn/colemanite surface due to the specific adsorption of Al^{3+} ions. With the addition of OH^- ions into the dispersion medium, starting from the initial pH of 6.8, the ζ potential shifted to the more negative regions. This may be explained by the increased amount of negative charge (OH^- ions) in the dispersion medium.

When the effects of various anionic electrolytes on ζ-potential values of PIn/colemanite dispersions were investigated, $\zeta_{Cl^-} = -1.6$ mV and $\zeta_{SO_4^{2-}} = -8.7$ mV (Figure 10b) were obtained at the initial pH of 6.8.
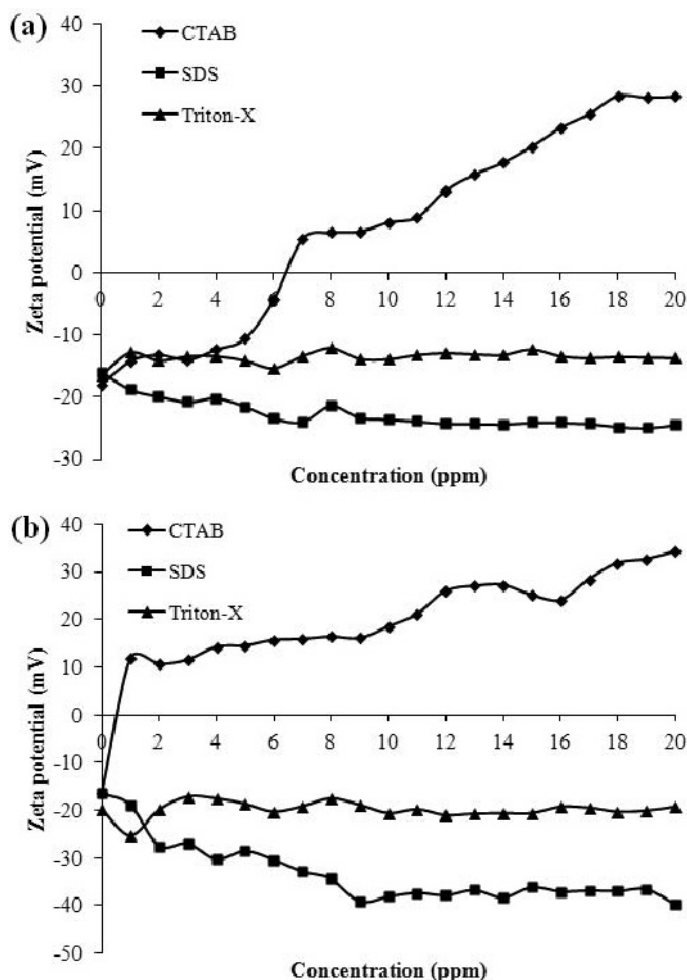

Figure 11. Effect of surfactants on the ζ potentials of (a) colemanite and (b) PIn/colemanite.

Divalent anions shifted these values to more negative regions than monovalent anions, which indicates an increased thickness in the electrical double layer. A similar behavior was reported in studies carried out on a polythiophene/borax conducting composite (Gumus *et al.*, 2011) and on ceramic membranes (made of alumina) (Zhao *et al.*, 2005).

Effect of surfactants on ζ. The ζ-potential values of colemanite and PIn/colemanite dispersions were observed to shift to more positive and negative regions with the addition of even small amounts of CTAB and SDS surfactants, respectively; whereas, almost no change was observed with the addition of Triton-X100 (Figure 11a,b).

When CTAB was added to the colemanite dispersion medium, the negatively charged surfaces of colemanite particles were covered by the positively charged (quaternary ammonium ions) hydrophilic heads of CTAB ions (Figure 11a). With the addition of more CTAB ions, the hydrophobic tails interacted with each other by means of Van der Waals interactions. The positively charged heads reoriented to remain on the surfaces of colemanite particles and, thus, shifted the ζ-potential values to more positive regions (Figure 12a)

and the ζ-potential value reached 28.3 mV at $c_{CTAB} = 20$ ppm. When SDS was added to the colemanite dispersion medium, the anionic head of the SDS surfactant interacted with Ca^{2+} ions on the surface of colemanite particles and the hydrophobic tail of the SDS, as in the case of CTAB, remained on outer surfaces. With the addition of more SDS, the tails interacted with each other and the negatively charged heads reoriented to remain on the surfaces. This shifted the ζ-potential values to more negative regions (Figure 12b) and the ζ-potential values reached 24.5 mV at $c_{SDS} = 20$ ppm. During the addition of the non-ionic surfactant, Triton-X100, the ζ-potential values of colemanite were virtually unchanged, at -13.5 mV and at $c_{Triton-X\ 100} = 20$ ppm.

The surfaces of PIn/colemanite composite particles were covered with the positively charged ionic part of the surfactant with the addition of CTAB and the ζ-potential value reached 34.2 mV at $c_{CTAB} = 20$ ppm (Figure 11b). When the anionic surfactant SDS was added to the PIn/colemanite composite dispersion medium, the ζ-potential values shifted to more negative regions and reached -39.7 mV at $c_{SDS} = 20$ ppm. During the addition of non-ionic surfactant, the ζ-potential values were ~ -20 mV and almost no change was

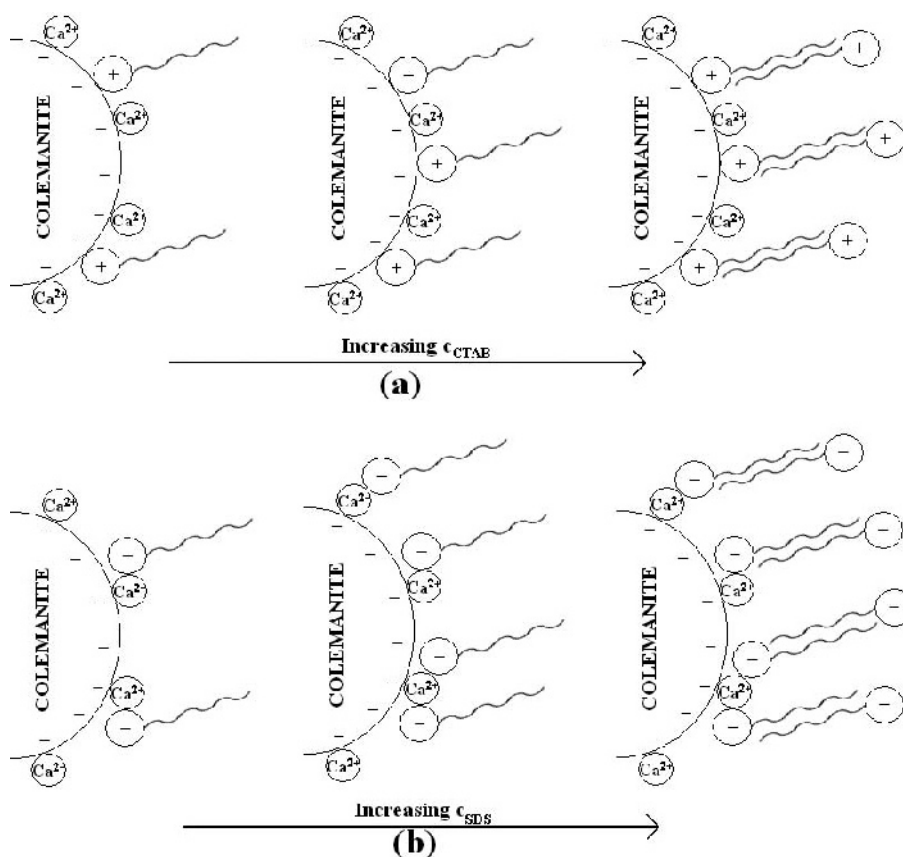
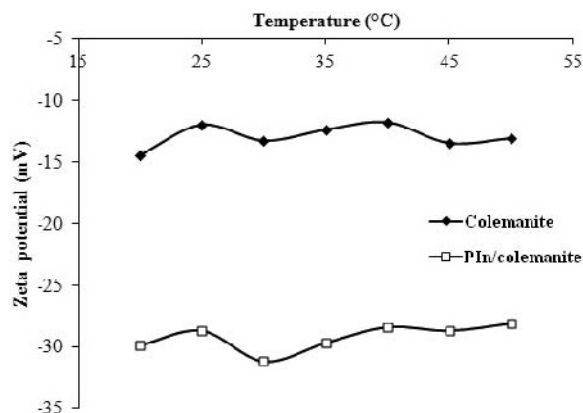Figure 12. Schematic representation of colemanite particles in water at different surfactant concentrations.

Figure 13. Effect of temperature on the ζ potentials of the samples.

observed even at $c_{Triton-X100} = 20$ ppm. Similar behaviors were reported by Ucar and Yargan (2009) for SDS and by Chotipong *et al.* (2007) for CTAB.

Effect of temperature on ζ potentials. Temperature has an effect on several parameters, including viscosity, dielectric constant, ion adsorption, conductivity, mobility of dispersed particles, and colloidal stability. Temperature also influences the surface potential of the colloidal particles because temperature can readily displace the equilibrium between the ionized groups and the medium (Garcia-Garcia *et al.*, 2004). At temperatures between 20 and 50ºC, however, the ζ potentials of colemanite and PIn/colemanite dispersions showed almost no change (Figure 13). The ζ potentials were measured as -14.5 mV at 20ºC and -13.1 mV at 50ºC for colemanite and -29.9 mV at 20ºC and -28.1 mV at 50ºC for PIn/colemanite composite dispersions. According to equation 1, the ζ potential of the material is proportional to the viscosity of the medium and inversely proportional to the dielectric constant of the medium. For the systems investigated in the present study, the viscosity/dielectric constant ratio may not change with increasing temperature, thus keeping the ζ potential almost constant.

CONCLUSIONS

Synthesis of PIn and PIn/colemanite conducting composites was carried out by *in situ* oxidative polymerization and the products were characterized by various means. The ζ-potential values of colemanite and PIn/colemanite dispersions were determined in the presence of various electrolytes and surfactants. Monovalent and divalent cations (Na^+ and Ba^{2+}) and anions (Cl^- and SO_4^{2-}) were determined to be indifferent ions for these dispersions. A trivalent cation (Al^{3+}), however, was determined to be a potential-determining ion for colemanite and PIn/colemanite dispersions. The ζ-potential values of both dispersions shifted to more positive and

more negative regions with the addition of CTAB and SDS, respectively, whereas, addition of Triton-X100 had no effect. The ζ-potential values of both dispersions were unchanged by variations in temperature.

REFERENCES

Alkan, M., Demirbas, O., and Dogan, M. (2005) Electrokinetic properties of sepiolite suspensions in different electrolyte media. *Journal of Colloid and Interface Science*, **281**, 240−248.

Alp, I. (2008) Application of magnetic separation technology for the recovery of colemanite from plant tailings. *Waste Management and Research*, **26**, 431−438.

Atar, N. and Olgun, A. (2007) Removal of acid blue 62 on aqueous solution using calcinated colemanite ore waste. *Journal of Hazardous Materials*, **146**, 171−179.

Bozkurt, A., Akbulut, U., and Toppare, L. (1996) Conducting polymer composites polypyrrole/polyindene. *Synthetic Metals*, **82**, 41−46.

Cabuk, T.Z., Sari, B., and Unal, H.I. (2010) Preparation of novel polyindene/polyoxymethylene blends and investigation of their properties. *Journal of Applied Polymer Science*, **117**, 3659−3664.

Cakic, M.D., Nikolic, G.S., and Ilic, L.A. (2002) FTIR Spectra of iron(III) complexes with dextran, pullulan and inulin oligomers. *Bulletin of the Chemists and Technologists of Macedonia*, **21**, 135−146.

Celik, M.S. (2004) Electrokinetic behavior of clay surfaces. Pp. 57−89 in: *Clay Surfaces Fundamentals and Applications* (F. Wypych and K.G. Satyanarayana, editors). Elsevier, Amsterdam.

Celik, M.S. and Bulut, R. (1996) Mechanism of selective flotation of sodium-calcium borates with anionic and cationic collectors. *Separation Science and Technology*, **31**, 1817−1829.

Celik, M.S., Hancer, M., and Miller, J.D. (2002) Flotation chemistry of boron minerals. *Journal of Colloid and Interface Science*, **256**, 121−131.

Chotipong, A., Scamehorn, J.F., Rirksomboon, T., Chavadej, S., and Supaphol, P. (2007) Removal of solvent-based ink from printed surface of high density polyethylene bottles by alkyltrimetylammonium bromides: Effect of pH, temperature, and salinity. *Colloids and Surfaces A: Physicochemical and Engineering Aspects*, **297**, 163−171.

Davies, T.W., Colak, S., and Hooper, R.M. (1991) Boric acid production by the calcination and leaching of powdered colemanite. *Powder Technology*, **65**, 433−440.

Davis, J.A., James, R.O., and Leckie, J.O. (1978) Surface ionization and complexation at the oxide/water interface: I. Computation of electrical double layer properties in simple electrolytes. *Journal of Colloid and Interface Science*, **63**, 480−499.

Duman, O. and Tunc, S. (2009) Electrokinetic and rheological properties of Na-bentonite in some electrolyte solutions. *Microporous and Mesoporous Materials*, **117**, 331−338.

El-Desoky, M.M. (2003) DC conductivity and hopping mechanism in V_2O_5-B_2O_3-BaO glasses. *Physica Status Solidi A: Applications and Materials* Science, **192**, 422−428.

Eristi, C., Yavuz, M., Yilmaz, H., Sari, B., and Unal, H.I.

(2007) Synthesis, characterization and electrorheological properties of polyindene/kaolinite composites. *Journal of Macromolecular Science Part A: Pure and Applied Chemistry*, **44**, 759−767.

Garcia-Garcia, S., Jonsson, M., and Wold, S. (2004) Temperature effect on the stability of bentonite colloids in water. *Journal of Colloid and Interface Science*, **298**, 694−705.

Gemici, U., Tarcan, G., Helvaci, C., and Somay, A.M. (2008) High arsenic and boron concetration in groundwaters related to mining activity in the Bigadic borate deposits. *Applied Geochemistry*, **23**, 2462−2476.

Gregory, J. (1989) Fundamental of flocculation. *Critical Reviews in Environmental Control*, **13**, 185−230.

Gumus, O.Y., Unal, H.I., Erol, O., and Sari, B. (2011) Synthesis, characterization, and colloidal properties of polythiophene/borax conducting composite. *Polymer Composites*, **32**, 418−426.

Gur, A. (2007) Dissolution mechanism of colemanite in sulphuric acid solutions. *Korean Journal of Chemical Engineering*, **24**, 588−591.

Gupta, S.K. and Stewart, H.W.B. (1975) The extraction and determination of plant-available boron in soils: *Schweizerische Landwirtschaftliche Monatshefte*, **14**, 153−169.]

Guzel, S., Unal, H.I., Erol, O., and Sari, B. (2012) Polyindene/organo-montmorillonite conducting nanocomposites I: Synthesis, characterization and electrokinetic properties. *Journal of Applied Polymer Science*, **123**, 2911−2922.

Hancer, M. and Celik, M.S. (1993) Flotation mechanisms of boron minerals. *Separation Science Technology*, **28**, 1703−1714.

Hang, J.Z., Zhang, Y.F., Shi, L., and Feng, Y. (2007) Electrokinetic properties of barite nanoparticles suspensions in different electrolyte media. *Journal of Materials Science*, **42**, 9611−9616.

Ishikawa, Y., Katoh, Y., and Ohshima H. (2005). Colloidal stability of aqueous polymeric dispersions: Effect of pH and salt concentration. *Colloids and Surfaces B: Biointerfaces*, **42**, 53−58.

Kanaoka, S., Ikeda, N., Tanaka, A., Yamaoka, H., and Higashimura, T. (2002) Cationic copolymerization of indene with styrene derivatives: synthesis of random copolymers of indene with high molecular weight. *Journal of Polymer Science Part A: Polymer Chemistry*, **40**, 2449−2457.

Kavas, T., Christogerou, A., Pontikes, Y., and Angelopoulos G.N. (2011) Valorisation of different types of boron-containing wastes of the production of lightweight aggregates. *Journal of Hazardous Materials*, **185**, 1381−1389.

Kaynak, C. and Isitman, N.A. (2011) Synergistic fire retardancy of colemanite, a natural hydrated calcium borate, in high-impact polystyrene containing brominated epoxy and antimony oxide. *Polymer Degradation and Stability*, **96**, 798−807.

Kennedy, J.P., Midha, S., and Keazler, B. (1993) Living carbocationic polymerization. 55. Living polymerization of indene. *Macromolecules*, **26**, 424−428.

Lee, D., Omolade, D., Cohen R.E., and Rubner, M.F. (2007) pH-dependent structure and properties of TiO_2/SiO_2 nanoparticle multi layer thin films. *Chemistry of Materials*, **19**, 1427−1433.

Lu, X., Zhang, W., Wang, C., Wen, T., and Wei, Y. (2011) One-dimensional conducting polymer nanocomposites: Synthesis, properties and applications. *Progress in Polymer Science*, **36**, 671−712.

MacDiarmid, A.G. (2001) Synthetic metals: A novel role for organic polymers. *Angewandte Chemie-International Edition*, **40**, 2581−2590.

Matejovic, I. (1993) Determination of carbon, hydrogen, and nitrogen in soils by automated elemental analysis (dry combustion method). *Communications in Soil Science and Plant Analysis*, **24**, 2213−2222.

Mitzi, A.B. (2001) Thin-film deposition of organic-inorganic hybrid materials. *Chemistry of Materials*, **13**, 3283−3298.

Oyhenart, L., Vigneras, V., Demontoux, F., and Parneix, J.P. (2005) A three-dimensional planar photonic crystal using conducting polymers. *Microwave and Optical Technology Letters*, **44**, 460−463.

Ozdemir, O. and Celik, M.S. (2010) Surface properties and flotation characteristics of boron minerals. *The Open Mineral Processing Journal*, **3**, 2−13.

Park, E.H., Jeong, S.U., Jung, U.H., Kim, S.H., Lee, J., Nam, S.W., Lim, T.H., Park, Y.J., and Yu, Y.H. (2007) Recycling of sodium metaborate to borax. *International Journal of Hydrogen Energy*, **32**, 2982−2987.

Parks, G.A. (1965) The isoelectric points of solid oxides, solid hydroxides and aqueous hydroxo complex systems. *Chemical Reviews*, **65**, 177−198.

Pavlyukevich, Y.G., Levitskii, I.A., and Mazura, N.V. (2009) Use of colemanite in class fiber production. *Glass and Ceramics*, **66**, 9−10.

Rao, S.R. (2004) Mechanism of the action of modifying agents. *Surface Chemistry of Forth Flotation: Reagents and Mechanisms*, Luwer Academic/Plenum Publishers, New York, 223 pp.

Sabaa, M.W., Mikhael, M.G., Furuhata, K., and Elsabee, M.Z. (1989) Thermal degradation behaviour of acrylonitrile-indene copolymers. *Polymer Degradation and Stability*, **23**, 257−269.

Sahinkaya, H.U. and Ozkan, A. (2011) Investigation of shear flocculation behaviors of colemanite with some anionic surfactants and inorganic salts. *Separation and Purification Technology*, **80**, 131−139.

Sari, A. and Tuzen, M. (2009) Kinetic and equilibrium studies of Pb(II) and Cd(II) removal from aqueous solutions onto colemanite ore waste. *Desalination*, **249**, 260−266.

Soga, K. and Monoi, T. (1989) Copolymerization of styrene with indene by the $Ti(OiPr)_4$-methylaluminoxane catalysts. *Macromolecules*, **22**, 3823−3824.

Stamm, M., editor (2008) *Polymer Surfaces and Interfaces: Characterization, Modification and Applications*. Polymer Science series, Springer-Verlag, Berlin, Heidelberg, 324 pp.

Tang, Y.F., Huang, Z.P., Feng, L., and Chen, Y.F. (2005) Fabrication of alpha-AlO(OH)-SiO_2 with core-shell structures by heterogeneous nucleation-and-growth processing. *Applied Surface Science*, **241**, 412−415.

Tkachenko, N.H., Yaremko, Z.M., and Bellmann, C. (2006) Effect of 1-1-charged ions on aggregative stability and electrical surface properties of aqueous suspensions of titanium dioxide. *Colloids and Surfaces A: Physicochemical and Engineering Aspects*, **279**, 10−19.

Ucar, A. and Yargan, M. (2009) Selective separation of boron values from the tailing of a colemanite processing plant. *Separation and Purification Technology*, **68**, 1−8.

Ulgut, B., Grose, J.E., Kiya, Y., Ralph, D.C., and Abruna, H.D. (2009) A new interpretation of electrohemical impedance spectroscopy to measure accurate doping level for conducting polymers: Separating Faradaic and capacitve currents. *Applied Surface Science*, **256**, 1304−1308.

Van der Pauw, L.T. (1958) A method of measuring specific resistivity and Hall effect of disc of arbitrary shape. *Philips Research Reports*, **13**, 1−9.

Yalcinkaya, O., Kalfa, O.M., and Turker, A.R. (2010) Chelating agent free solid phase extraction (CAF-SPE) method for separation and/or preconcentration of iron(III) ions. *Turkish Journal of Chemistry*, **34**, 207−217.

Waclawska, I. and Stoch, L. (1988) Thermal decomposition of colemanite. *Thermochimica Acta*, **126**, 307−318.

Walcarius, A. (2001) Electrochemical applications of silica-based organic-inorganic hybrid materials. *Chemistry of Materials*, **13**, 3351−3372.

Weir, C.E. (1966) Infrared spectra of the hydrated borates. *Journal of Research of the National Bureau of Standards − A. Physics and Chemistry*, **70A**, 153−164.

Zhao, Y., Xing, Y.Z.W., Xu, N., and Wong, F.S. (2005) Effects of inorganic electrolytes on zeta potentials of ceramic microfiltration membranes. *Separation and Purification Technology*, **42**, 117−121.